

Search for heavy Majorana neutrinos at electron-proton colliders

Haiyong Gu^{1,*} and Kechen Wang^{1,†}

¹*Department of Physics, School of Science, Wuhan University of Technology,
430070 Wuhan, Hubei, China*

We develop the search strategy for a heavy Majorana neutrino via the lepton number violation signal process $pe^- \rightarrow \mu^+ jjj$ at future electron-proton colliders. The signal and dominant standard model background events are generated with the fast detector simulation. We apply the pre-selection criteria and perform the multi-variate analysis based on machine-learning to reject the background. Distributions of representative kinematic observables are presented for both signal and background processes and effects on final limits are compared by inputting two different set of observables when performing multi-variate analysis. The 2- and 5- σ limits on the mixing parameter $|V_{\ell N}|^2$ are predicted for the heavy neutrino mass m_N in the range of 10–1000 GeV. At the LHeC (FCC-eh) with an electron beam energy of 60 GeV, a proton beam energy of 7 (50) TeV and an integrated luminosity of 1 (3) ab^{-1} , the mixing parameter $|V_{\ell N}|^2$ can be constrained to be below ~ 3.0 (1.0) $\times 10^{-6}$ for m_N around $\mathcal{O}(100)$ GeV at 2- σ level. The limits are much stronger than the current experiment limits at the LHC for m_N above 30 GeV. The positron signal final state and the effect of long-lived cases of heavy neutrinos are also checked and commented.

I. INTRODUCTION

The neutrino oscillation experiments [1–6] have proved that neutrinos in standard model (SM) have very tiny masses. Because of the lack of right-handed neutrinos in the SM, the Dirac mass terms cannot be formed as other fermions in the Lagrangian and the SM needs to be extended to explain their non-zero masses. One important solution is the seesaw mechanism [7–17], where new gauge singlet right-handed neutrinos N_R are introduced and masses of active neutrinos are generated by mixing SM left-handed neutrinos ν_L with right-handed neutrinos N_R , resulting in heavy mass eigenstates N that have small SM ν_L components. Therefore, searches for heavy neutrinos are crucial to verify the seesaw mechanism and explore the origin of neutrino masses.

At colliders, such heavy neutrinos are usually also called heavy neutral leptons and are extensively searched relying on their effective couplings to SM gauge bosons via their mixing with SM neutrinos. In theory, the production cross section, decay width, and lifetime of N depend on its mass m_N and the parameter $|V_{\ell N}|^2$ which is related to the matrix element describing the mixing of N with the SM neutrino of flavor ℓ . Therefore, limits for such searches are usually given in the plane of the mixing parameter $|V_{\ell N}|^2$ vs. the heavy neutrino mass m_N . Summaries of collider searches of heavy neutrinos can be found in Refs. [18–23] and references therein.

Refs. [24–31] are recent experimental studies on heavy neutrino searches. Among them, the CMS collaboration has analyzed the data with center-of-mass energy $\sqrt{s} = 13$ TeV and an integrated luminosity of 35.9 fb^{-1} [24, 25] and 137 fb^{-1} [26]. Ref. [24] searched for a heavy Majorana neutrino in the trilepton signal process $pp \rightarrow W^{(*)} \rightarrow \ell N \rightarrow \ell(\ell W^{(*)}) \rightarrow \ell(\ell\ell\nu)$ and limits are applied on both $|V_{eN}|^2$ and $|V_{\mu N}|^2$ for the heavy neutrino mass range between 1 GeV and 1.2 TeV. Ref. [25] searched for a heavy Majorana neutrino in the same-sign dilepton channel $W^{(*)} \rightarrow \ell^\pm N \rightarrow \ell^\pm(\ell^\pm W^{(*)}) \rightarrow \ell^\pm(\ell^\pm jj)$. The upper limits are set on $|V_{eN}|^2$, $|V_{\mu N}|^2$, and $|V_{eN}V_{\mu N}^*|^2/(|V_{eN}|^2 + |V_{\mu N}|^2)$ for N masses between 20 and 1600 GeV. Ref. [26] searched for a long-lived heavy neutrino of either Majorana or Dirac type in the signal process $pp \rightarrow W \rightarrow \ell N \rightarrow \ell(\ell W^*/\nu Z^*) \rightarrow \ell\ell\ell\nu$. The final state consists of three leptons among which two leptons form a displaced vertex with respect to the primary proton-proton collision vertex and the third lepton emerges from the primary vertex. Limits are applied on $|V_{eN}|^2$ and $|V_{\mu N}|^2$ in the mass range between 1 and 15 GeV.

In Ref. [27], a heavy Majorana neutrino was investigated by the ATLAS collaboration in the similar signal process to that in Ref. [24]. Data at $\sqrt{s} = 13$ TeV and integrated luminosity of 36.1 (32.9) ab^{-1} are analysed for the prompt (displaced) leptonic decay case. Constraints on $|V_{eN}|^2$ and $|V_{\mu N}|^2$ are set for heavy neutrino mass in the range of 4.5 to 50 GeV. The LHCb collaboration searched for a heavy Majorana neutrino in the signal process $W^+ \rightarrow \mu^+ N \rightarrow \mu^+(\mu^\pm jj)$ [28]. Data corresponding to an integrated luminosity of 3.0 fb^{-1} and

* haiyong.gu@whut.edu.cn

† kechen.wang@whut.edu.cn (Corresponding author)

center-of-mass energies of 7 and 8 TeV are analysed and upper limits on $|V_{\mu N}|^2$ are set to be $\sim 10^{-3}$ (10^{-4}) in the mass range from 5 to 50 GeV for the lepton number conserving (violating) case.

The NA62 collaboration searched for N produced from $K^+ \rightarrow e^+ N$ decays and placed the upper limit on $|V_{eN}|^2 \sim 10^{-9}$ in the mass range 144–462 MeV [29]. Heavy neutrinos from B-meson decays are investigated by the Belle collaboration and upper limits are set on $|V_{eN}|^2$, $|V_{\mu N}|^2$, $|V_{eN}||V_{\mu N}|$ in the mass range 0.5–5.0 GeV [30]. The T2K Collaboration searched for heavy neutrinos from kaon decays and constrained mixing parameters $|V_{\ell N}|^2$ with $\ell = e, \mu, \tau$ for m_N between 140 and 493 MeV [31]. Moreover, for N produced from meson decays, the SHiP collaboration’s search prospect for long-lived neutrinos predicts strong sensitivity on $|V_{\ell N}|^2$ with $\ell = e, \mu, \tau$ flavors for m_N in the range 0.1 – 5.8 GeV [32]. The combination of electroweak precision observables and lepton flavor violating decays can also set constraints indirectly on mixing parameters $|V_{\ell N}|^2$, especially when m_N is larger than 80 GeV [33].

In this article, we develop the search strategy for a heavy Majorana neutrino via the lepton number violation (LNV) signal process of $p e^- \rightarrow \mu^+ jjj$ at future electron-proton colliders, the Large Hadron electron Collider (LHeC) [34–39] and the electron-hadron mode of the Future Circular Collider (FCC-eh) [37, 39–42]. We consider the LHeC (FCC-eh) running with an electron beam energy of 60 GeV and a proton beam energy of 7 (50) TeV, which corresponds to $\sqrt{s} = 1.3$ (3.5) TeV. The integrated luminosities are assumed to be 1 and 3 ab^{-1} at the LHeC and FCC-eh, respectively.

Compared with the proton colliders, such as the high-luminosity LHC (HL-LHC), the centre-of-mass energy of ep colliders is lower. However, due to lack of gluon-exchange diagrams, the SM QCD backgrounds, which are dominant at pp colliders, are much smaller at ep colliders. Besides, the number of additional interactions in the same event (pileup) is negligible at ep colliders, while it is expected to be very large at the HL-LHC. Furthermore, heavy neutrinos with mass above 100 GeV can still be produced on-shell from the t -channel exchange of W -boson at ep colliders, while at the HL-LHC such heavy neutrinos are produced from off-shell W - or Z -boson processes with limited cross section. Therefore, future ep colliders could be complementary to the pp collider when searching for beyond standard model (BSM) physics scenarios, particularly for heavy neutrinos.

Ref. [43] and references therein have reviewed BSM physics searches at the LHeC and FCC-eh, while phenomenology studies on heavy neutrino searches at ep

colliders can be found in Refs. [44–57]. Among them, Ref. [50] investigated heavy Majorana neutrinos produced in an effective Lagrangian approach at the LHeC. For the LHeC, they considered a 7 TeV proton beam colliding with an electron beam of two energies: $E_e = 50$ and 150 GeV. The events are simulated at the parton level and kinematic cuts are applied to reduce the background. Limits are placed on the neutrino mass and the effective coupling. Ref. [51] explored heavy neutrinos at the LHeC in the context of an inverse-seesaw model. The production cross section of various signals of Nj , NjW^- and e^-jW^- are calculated with and without 80% left-polarized electron beam. The events are simulated at the parton level and kinematic cuts are applied to reduce the background. The required integrated luminosities are estimated to achieve a 3- σ statistical significance for two different heavy neutrino masses of 150 and 400 GeV. Ref. [54] searched for heavy Majorana neutrino via the signal processes $p e^- \rightarrow e^- \mu^\pm \mu^\pm + X$ and $p e^- \rightarrow \nu_e \mu^- \mu^\pm + X$. The events are simulated including detector smearing effects and kinematic cuts are applied to reduce the background. The required integrated luminosities are estimated for heavy neutrino masses in the range of 100 and 1000 GeV. Ref. [55] investigated a heavy neutrino via the signal process $p e^- \rightarrow jN \rightarrow j(e^\pm W^\mp) \rightarrow j(e^\pm J)$, where J is a fat-jet from a highly boosted W -boson. The events are simulated at the parton level and passed through selection cuts to reduce the background. Bounds on $|V_{eN}|^2$ are placed for m_N in the range of 400 to 1000 GeV. Ref. [56] probed heavy neutrinos via the lepton flavor violating signal process $p e^- \rightarrow jN \rightarrow j(\mu^- W^+) \rightarrow \mu^- + 3j$ at the LHeC and FCC-eh. Background processes include $j e^- VV$ and $j \nu_e VV$ where $V = Z, W^\pm$ and $VV \rightarrow (jj)(\mu^- \mu^+ / \mu^- \bar{\nu}_\mu)$. Limits on the mixing parameters $|\theta_e \theta_\mu|$ are placed for the heavy neutrino mass in the range from 100 to 1000 GeV.

We note that this work is different from all previous phenomenology studies due to the combination of following aspects: (i) we consider the LNV signal process $p e^- \rightarrow \mu^+ + jjj$ assuming $|V_{\ell N}|^2 = |V_{eN}|^2 = |V_{\mu N}|^2$ in the context of a simplified Type-I seesaw model; (ii) SM background includes four inclusive processes listed in Table I; (iii) for both the signal and background event simulation, we utilize the program chain including the event generator, parton shower, hadronization and detector effects; (iv) for the LHeC (FCC-eh), we consider a 60 GeV electron beam colliding with a proton beam of 7 (50) TeV energy and an integrated luminosity of 1 (3) ab^{-1} ; (v) we apply pre-selection criteria and perform multi-variate analysis based on machine-learning to reject the background; (vi) The 2- and 5- σ limits on the

mixing parameter $|V_{\ell N}|^2$ are predicted for the heavy neutrino mass in the range 10–1000 GeV.

The article is organised as follows. Sec. II presents the data simulation and the cross section of the signal process. Sec. III describes the SM background processes and our search strategy. The analysis details and limits on the mixing parameters $|V_{\ell N}|^2$ at both the LHeC and FCC-eh are shown in Sec. IV. We summarize our study, and comment on the effect of long-lived cases of heavy neutrinos and the positron signal final state in Sec. V.

II. THE LNV SIGNAL

To simplify the analyses, we consider the Type-I seesaw model and assume that there is only one generation of heavy neutrinos N which mixes with active neutrinos of electron and muon flavours with the same mixing parameters, i.e. $|V_{\ell N}|^2 = |V_{eN}|^2 = |V_{\mu N}|^2$. We also assume that N decays promptly in this study. As shown in Fig. 1, the heavy Majorana neutrino N can be produced via the t -channel exchange of W -boson at ep colliders, and finally decay into μ^+ plus three jets. The lepton number of this process changes from +1 to -1 , so it violates the conservation of lepton number.

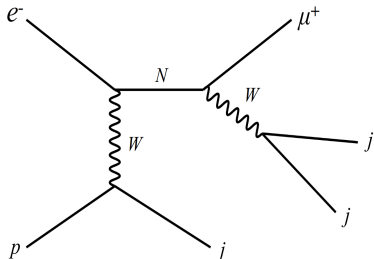


FIG. 1: The production process of the LNV signal via a Majorana heavy neutrino N at ep colliders.

For the data simulation, we implement the Universal FeynRules Output model file [58, 59] which extends the SM with additional heavy neutrinos interacting with active neutrinos, into the MadGraph5 [60] to generate the signal events. Similar to our previous work [61], the Pythia6 [62] program is modified to perform the parton showering and hadronization for ep colliders, while the configuration card files [63] for the LHeC and FCC-eh detectors are implemented to the Delphes program [64] to complete the detector simulation.

To maintain consistency throughout this study, the production cross sections calculated by MadGraph5 are used to estimate the number of events for both signal and background processes. In Fig. 2, we plot the cross

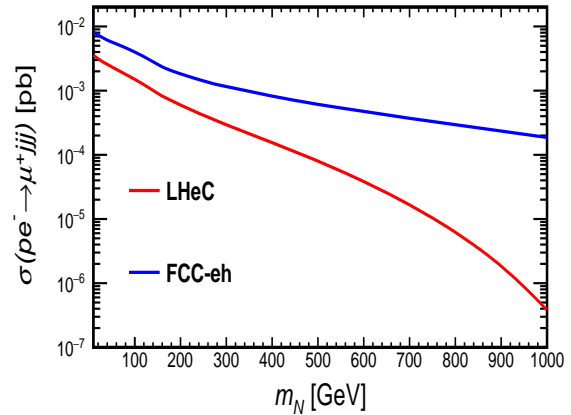


FIG. 2: The production cross section of the LNV signal $pe^- \rightarrow \mu^+ jjj$ via the heavy Majorana neutrino N for varying heavy neutrino masses m_N at the LHeC and FCC-eh with $|V_{\ell N}|^2 = 10^{-4}$.

sections of the LNV signal $pe^- \rightarrow \mu^+ jjj$ via the heavy Majorana neutrino N as a function of the heavy neutrino mass m_N at the LHeC and FCC-eh, where the mixing parameter $|V_{\ell N}|^2$ is fixed to be 10^{-4} .

For large m_N , cross sections at the LHeC decrease much faster than those at the FCC-eh. This behaviour can be understood from the parton distribution function (PDF) of the proton. In this study, heavy neutrinos are produced from the t -channel W -boson exchange process $qe^- \rightarrow jN$. In order to produce heavy neutrinos with large mass, momenta of incoming quarks need to be large enough, so that the centre of mass energy $\sqrt{s} = 2\sqrt{E_e E_q}$ is larger than m_N . Considering a quark carries a fraction x of the longitudinal momentum of a proton, only quarks with $x \gtrsim m_N^2/(4E_e E_p)$ can contribute to the signal production cross section. Since the parton density function $f(x)$ of the quark decreases rapidly for large x values [65], when m_N is very large, the number of quarks which satisfies the condition $x \gtrsim m_N^2/(4E_e E_p)$ becomes tiny. This leads to the rapid decrease in the production cross section for large m_N .

III. BACKGROUND AND SEARCH STRATEGY

Since the signal process $pe^- \rightarrow \mu^+ jjj$ violates the lepton number conservation explicitly, it has little SM background in theory. Considering the signal final state contains one positive charged muon plus multi-jets, there are mainly four SM background processes, which we label as “B1 - B4” in this article. We list their production cross sections in Table I. They can contribute to the back-

ground when the final state e^- and/or μ^- are undetected. Among these four background processes, $\mu^+\mu^-e^-jjj$ and $\mu^+\nu_\mu e^-jjj$ have large cross sections and are more difficult to eliminate. We note that the considered four background processes have both QED and QCD interactions. Processes with pure QED interactions are checked and the sum of their cross sections are found to be only a factor of about 1/90 (1/45) of the considered background at the LHeC (FCC-eh). Because they are much smaller and our computing resources are limited, we do not include the background processes with only QED interactions.

σ [pb]	LHeC	FCC-eh
B1 $\mu^+\mu^-e^-jjj$	0.58	2.1
B2 $\mu^+\mu^-\nu_ejjj$	8.6×10^{-2}	0.39
B3 $\mu^+\nu_\mu e^-jjj$	0.28	1.6
B4 $\mu^+\nu_\mu\nu_ejjj$	8.1×10^{-6}	9.3×10^{-5}

TABLE I: The production cross sections of dominant background processes at the LHeC and FCC-eh.

The final state muon can also come from tau decays. However, it will not contribute too much to the background because of the following two reasons: (i) the small tau to muon branching ratio; (ii) the leptonic decay of taus produce neutrinos, resulting in large missing energy in the final state, and cannot pass our missing energy pre-selection cut. We checked four background processes $\tau^+\tau^-e^-jjj$, $\tau^+\tau^-\nu_ejjj$, $\tau^+\nu_\tau e^-jjj$, and $\tau^+\nu_\tau\nu_ejjj$ at the LHeC (FCC-eh) and found that after pre-selection the event rate of total background increased only by a factor of 6% (11%). After performing the full analysis described below, we find that after adding the tau background, the limit on $|V_{\ell N}|^2$ changed from $3.6 (1.10)\times 10^{-6}$ to $3.8 (1.12)\times 10^{-6}$ for the benchmark $m_N = 120$ GeV. Since the effects on the limits are very small, we did not add the tau background in this study.

We apply the following pre-selection cuts to select the signal and reject the background events at the first stage. (i) Exactly one muon with positive charge, i.e. $N(\mu^+) = 1$ and transverse momentum $p_T(\mu) > 5$ GeV; events with final state electron(s) or tau(s) are vetoed. (ii) All jets are sorted in descending order according to their transverse momenta and we require at least three jets, i.e. $N(j) \geq 3$; for the p_T thresholds of jets, when heavy neutrino mass is below 80 GeV, the p_T of the first three leading jets are required to be greater than 10 GeV, while when masses are above 80 GeV, we require the first two leading jets to have p_T greater than 20 GeV and the third one to have p_T greater than 10 GeV. (iii) Since both the final state

neutrinos and the missing of leptons contribute to the missing energy, the background has much larger missing energy compared with the signal and a pre-selection of missing energy $\cancel{E}_T < 10$ GeV is applied to reject the background.

For the signal data simulation, we vary the heavy neutrino mass m_N from 10 to 1000 GeV and generate 0.3 million signal events at the LHeC and FCC-eh for each m_N . Due to limited computational resources, we are not able to generate huge number of events for every background processes. The number of simulated events for each background process is determined according to its importance in reducing the statistical uncertainty on final limits. For the background, we generate 2.1 (2.0) million $\mu^+\mu^-e^-jjj$, 10.5 (6.0) million $\mu^+\mu^-\nu_ejjj$, 27.4 (24.6) million $\mu^+\nu_\mu e^-jjj$ and 6.0 (6.4) million $\mu^+\nu_\mu\nu_ejjj$ events at the LHeC (FCC-eh), respectively. In Table II, we show the number of events for the signal with benchmark $m_N = 120$ GeV and four background processes after applying the pre-selection cuts (i)-(iii) sequentially described above.

		signal	B1	B2	B3	B4
LHeC	initial	1.2×10^3	5.8×10^5	8.6×10^4	2.8×10^5	8.1
	(i)	1.1×10^3	2.6×10^3	4.0×10^3	1.9×10^4	6.2
	(ii)	853	799	1.3×10^3	6.5×10^3	4.4
	(iii)	702	699	9.3	154	0.1
FCC-eh	initial	1.0×10^4	6.2×10^6	1.2×10^6	4.9×10^6	278
	(i)	8.8×10^3	1.3×10^4	6.1×10^4	2.8×10^5	118
	(ii)	7.2×10^3	4.1×10^3	2.3×10^4	1.2×10^5	99
	(iii)	5.5×10^3	2.8×10^3	125	3.2×10^3	1.2

TABLE II: The number of events for the signal with benchmark $m_N = 120$ GeV and four background processes after applying pre-selection cuts (i)-(iii) sequentially. The numbers correspond to the LHeC and FCC-eh with 1 and 3 ab^{-1} integrated luminosity, respectively.

To further reject the background, we input the following nineteen observables into the TMVA [66] package to perform the multivariate analysis (MVA).

- A. The four-momenta of the final state muon: $E(\mu)$, $p_x(\mu)$, $p_y(\mu)$, $p_z(\mu)$.
- B. The number of jets $N(j)$ and the four-momenta of the first three leading jets: $E(j_1)$, $p_x(j_1)$, $p_y(j_1)$, $p_z(j_1)$; $E(j_2)$, $p_x(j_2)$, $p_y(j_2)$, $p_z(j_2)$; $E(j_3)$, $p_x(j_3)$, $p_y(j_3)$, $p_z(j_3)$.
- C. The magnitude and the azimuthal angle of the

missing transverse momentum: $\cancel{E}_T, \phi(\cancel{E}_T)$;

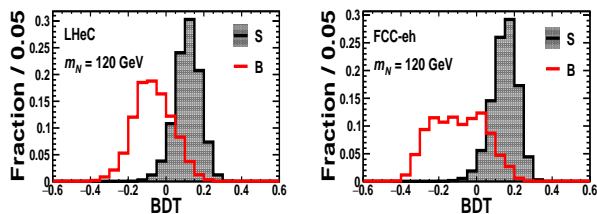


FIG. 3: Distributions of BDT responses for the signal with $m_N = 120$ GeV (black, filled) and total SM background (red) at the LHeC (left) and FCC-eh (right).

The Boosted Decision Tree (BDT) method in the TMVA package is adopted to separate the background from the signal. Fig. 3 shows the BDT distributions for the total background and the benchmark signal with $m_N = 120$ GeV at the LHeC and FCC-eh. The BDT distributions of the signal and background are well separate, which means that a BDT cut can be applied to reject the background. Comparing left and right plots, one sees that the signal distributions of LHeC and FCC-eh are similar, but the background distribution of LHeC has an obvious peak, while the background distribution of FCC-eh is flatter. In addition, the distributions of signal and background overlap slightly less at the FCC-eh, indicating that the separation between the signal and background is better than LHeC.

Since the kinematics of the signal varies with m_N , the distributions of BDT response also change with m_N . In Figs. 6 and 7, we show the BDT distributions of four background processes and the signal corresponding to more representative heavy neutrino masses at the LHeC and FCC-eh. We observe that as m_N increases, the signal and background B1 ($\mu^+\mu^-e^-jjj$) become more separate. However, the signal and the other three backgrounds overlap more and more as m_N changes from 20 to 200 GeV, and then separate more and more as m_N changes from 200 GeV to 1 TeV. When $m_N = 1$ TeV, BDT distributions of all background processes tend to be similar and are almost completely separate from the signal. However, the limit for $m_N = 1$ TeV is still restricted by its small signal cross section. We note that when the kinematical distributions of background and signal are similar, it is difficult to distinguish between the signal and background, leading to large overlap between their BDT distributions. Therefore, the extent of separation between the BDT distributions of signal and background are determined by the degree of deviation of

their kinematics.

We note that the above input observables including the four-momenta and angles are very basic and usually called low-level variables for the MVA analysis. One can also construct some complicated observables and input such high-level variables to perform the MVA analysis. To compare the effects on the final limits by inputting different sets of variables, we construct twenty-nine high-level observables and show the distributions of eight representative ones for the signal with $m_N = 120$ GeV and four background processes at the LHeC and FCC-eh in Fig. 8 and Fig. 9. The representative observables are ordered according to the separation between the signal and background. At both colliders, the best observables to separate the signal from background are $p_T(\mu)$, $E(\mu)$ and $\eta(\mu)$. This is mainly because the two main background processes B1 ($\mu^+\mu^-e^-jjj$, blue) and B3 ($\mu^+\nu_\mu e^-jjj$, pink) are well separate from the signal for these observables. One observes that the invariant mass $M(\mu + j_2 + j_3)$ can also be a good discriminator. This is because $M(\mu + j_2 + j_3)$ has a sharp peak around m_N , which means that it can also be used to reconstruct the heavy neutrino mass.

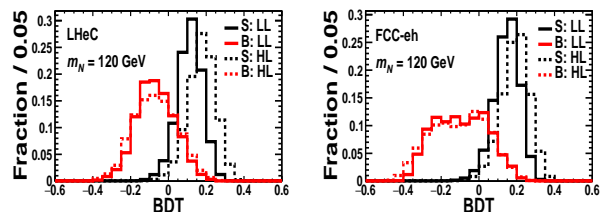


FIG. 4: Distributions of BDT responses for the signal with $m_N = 120$ GeV and total background when inputting high-level (HL, dashed) and low-level (LL, solid) observables at the LHeC (left) and FCC-eh (right).

Fig. 4 shows the distributions of BDT responses for the signal with $m_N = 120$ GeV and total background when inputting high-level (HL, dashed) and low-level (LL, solid) observables at the LHeC (left) and FCC-eh (right). One sees that the BDT distributions are similar between the low- and high-level cases. Although some high-level observables seem to separate the signal better from the background than low-level observables, each high-level observable is not independent of each other and has correlations. The MVA-BDT analysis combines the information from all input observables with correlations. Since two sets of low- and high-level observables contain similar information, their BDT distributions should be similar as well.

To estimate the effects on final limits, we complete the analyses for the benchmark $m_N = 120$ GeV using high-level observables at the LHeC (FCC-eh) and find that BDT cut efficiencies change from 7.71 (7.95) $\times 10^{-1}$ to 7.27 (7.20) $\times 10^{-1}$ for the signal and from 1.03×10^{-1} (8.85×10^{-2}) to 3.95 (3.17) $\times 10^{-2}$ for the total background. The final $2\text{-}\sigma$ limit decreases slightly from 3.6×10^{-6} to 2.4×10^{-6} for LHeC and from 1.1×10^{-6} to 7.3×10^{-7} for FCC-eh, respectively. Because the changes in the final results are small and more computing resources are needed to input more observables, for simplicity we input low-level variables to TMVA to obtain the results below.

IV. RESULTS

In this section, based on our analyses we show the limits on the mixing parameter $|V_{\ell N}|^2$ for the heavy neutrino mass m_N in the range of 10 to 1000 GeV. After the pre-selection, the BDT cut is optimized according to the signal statistical significance calculated by Eq. 1 for each mass case.

$$\sigma_{\text{stat}} = \sqrt{2[(N_s + N_b)\ln(1 + \frac{N_s}{N_b}) - N_s]}, \quad (1)$$

where N_s (N_b) is the number of signal (total background) events after all selection cuts.

In Table III, we show selection efficiencies of pre-selection and BDT cuts for both signal and background processes at the LHeC and FCC-eh for representative heavy neutrino masses. The total selection efficiency is the product of pre-selection and BDT cut efficiencies. The number of background events after all cuts can be calculated by multiplying the initial number in Table II by the total selection efficiency, while the number of signal events can be calculated as the product of signal cross section, collider luminosity and total selection efficiency.

In Fig. 5, we show 2- and $5\text{-}\sigma$ limits on mixing parameter $|V_{\ell N}|^2$ for the heavy neutrino mass in the range of 10 to 1000 GeV at the LHeC (FCC-eh) with an electron beam energy of 60 GeV, a proton beam energy of 7 (50) TeV and an integrated luminosity of 1 (3) ab^{-1} . At the LHeC, as m_N changes from 10 GeV to 100 GeV, the $2\text{-}\sigma$ upper limits on $|V_{\ell N}|^2$ decrease from 7.8×10^{-5} to 3.2×10^{-6} ; the limits are relatively flat for m_N between 100 GeV to 500 GeV and increase rapidly to 3.3×10^{-3} afterwards. The $2\text{-}\sigma$ limit at the FCC-eh has similar behavior as that at the LHeC, but its varying range is much smaller, between $\sim 10^{-6}$ and 10^{-5} . At both colliders, the $5\text{-}\sigma$ limits are slightly weaker than those for $2\text{-}\sigma$.

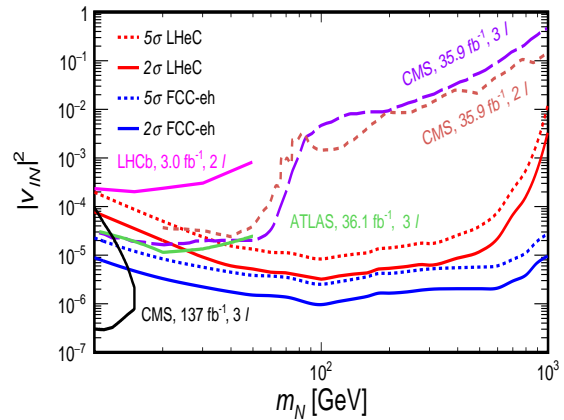


FIG. 5: 2- and $5\text{-}\sigma$ limits on mixing parameter $|V_{\ell N}|^2$ for the heavy neutrino mass in the range of 10 to 1000 GeV at the LHeC and FCC-eh. Also shown are the current experimental limits at 95% confidence level from the trilepton searches (CMS, 35.9 fb^{-1} , 3ℓ) [24], (CMS, 137 fb^{-1} , 3ℓ) [26], (ATLAS, 36.1 fb^{-1} , 3ℓ) [27] and dilepton searches (CMS, 35.9 fb^{-1} , 2ℓ) [25], (LHCb, 3.0 fb^{-1} , 2ℓ) [28] at the LHC.

The increasing or decreasing behavior of the upper limit is the result of the competition between the signal cross section and the separation extent of the signal and background kinematical distributions. With the increase of m_N , the signal cross section decreases gradually as shown in Fig. 2, while BDT distributions of the signal and the total background become more and more separate (cf. Figs. 6 and 7). Therefore, limits are weaker because of smaller separations between the signal and background kinematics for small masses and because of smaller signal cross sections for heavy masses. The most stringent limits are achieved at $m_N \sim 100$ GeV. Limits are relatively flat in the middle range of m_N because of the offset between the decrease of the signal cross section and increase of the separation extent of the signal and background kinematics. At the LHeC, when $m_N \gtrsim 500$ GeV, the signal cross section decreases rapidly with the increase of m_N , leading to the rapid increase in the upper limit. Since the signal cross section at the FCC-eh decreases slowly, the limit for heavy masses also increases gently. The FCC-eh has better limits than the LHeC, mainly because the signal cross section of FCC-eh is larger than that of LHeC for the same m_N .

To compare with current experiment limits, we also present the recent LHC limits in Fig. 5. The details of these studies are reviewed in Sec. I. The limit curve for (CMS, 35.9 fb^{-1} , 2ℓ) is reinterpreted from the origi-

nal limit on the parameter $|V_{eN}V_{\mu N}^*|^2/(|V_{eN}|^2 + |V_{\mu N}|^2)$ in the CMS same-sign dilepton search [25]. With the same assumption of $|V_{eN}|^2 = |V_{\mu N}|^2$ in this article, the original limit is shown by multiplying a factor of two. The limit for (CMS, 137 fb^{-1} , 3ℓ) is from the Ref. [26] where the CMS collaboration searched for a long-lived heavy neutrino in the trilepton final state with displaced vertices. It has excluded some parameter regions when $m_N < 15 \text{ GeV}$. Our analyses show that the LHeC limit is slightly weaker than the current CMS and ATLAS trilepton searches when $m_N \lesssim 20 \text{ GeV}$, while it is better for heavier masses and about two to three orders of magnitude stronger than the current CMS limits when $m_N \gtrsim 100 \text{ GeV}$. Compared with current LHC limits, the FCC-eh gives more stringent limits when $m_N > 15 \text{ GeV}$ and are much stronger when $m_N \gtrsim 100 \text{ GeV}$.

V. SUMMARY AND DISCUSSION

In this paper, we utilize the lepton number violation signal process of $pe^- \rightarrow \mu^+ jjj$ to search for heavy Majorana neutrinos at the future electron-proton colliders. We consider the LHeC (FCC-eh) running with an electron beam energy of 60 GeV, a proton beam energy of 7 (50) TeV and an integrated luminosity of 1 (3) ab^{-1} . To simplify the analyses, we consider the simplified Type-I model and assume that only one generation of heavy neutrinos N is within the collider access and mixes with active neutrinos of electron and muon flavours with the same mixing parameters, i.e. $|V_{\ell N}|^2 = |V_{eN}|^2 = |V_{\mu N}|^2$ and $|V_{\tau N}|^2 = 0$. The signal production cross sections are presented in Fig. 2 at both LHeC and FCC-eh for the heavy neutrino mass m_N in the range of 10–1000 GeV. We apply detector configurations and simulate signal and four dominant SM background events of $\mu^+\mu^-e^-jjj$, $\mu^+\mu^-e^-jjj$, $\mu^+\nu_e jjj$, $\mu^+\nu_\mu e^- jjj$ and $\mu^+\nu_\mu \nu_e jjj$ including detector effects.

We first use the pre-selection cuts to select the final state with exactly one muon with positive charge, at least three jets and small missing energy. The number of events for the signal with benchmark $m_N = 120 \text{ GeV}$ and four background processes after applying pre-selection cuts are presented in Table II. To reject the background efficiently, nineteen basic observables are input to perform the multi-variate analyses based on machine-learning. The distributions of BDT responses of the signal and the SM background processes at the LHeC and FCC-eh for representative heavy neutrino masses are shown in Appendix A, while the efficiencies of pre-selection and BDT cuts are shown in Appendix C.

To test the effects on the final limits by inputting different sets of observables, we construct and input another set of twenty-nine observables and find that the changes in the final limits are small. The distributions of eight high-level representative kinematic observables are also presented in Appendix B for the signal with $m_N = 120 \text{ GeV}$ and four background processes at the LHeC and FCC-eh.

Based on our analyses, we show the 2- and 5- σ upper limits on the mixing parameter $|V_{\ell N}|^2$ for the heavy neutrino mass m_N in the range of 10–1000 GeV at both LHeC and FCC-eh in Fig. 5. At the LHeC, the 2- σ upper limits on $|V_{\ell N}|^2$ decrease from 7.8×10^{-5} to 3.2×10^{-6} when m_N changes from 10 GeV to 100 GeV; the limits are relatively flat for m_N in the middle range between 100 GeV and 500 GeV and increase rapidly to 3.3×10^{-3} afterwards. The 2- σ limit at the FCC-eh has the similar behavior as that at the LHeC, but its varying range is much smaller, between $\sim 10^{-6}$ and 10^{-5} . At both colliders, the 5- σ limits are slightly weaker than those for 2- σ .

The limits are compared with the current LHC experimental limits. Our analyses show that the LHeC limit is slightly weaker than the current CMS and ATLAS trilepton searches when $m_N \lesssim 20 \text{ GeV}$, while it is better for heavier masses and about two to three orders of magnitude stronger than the current CMS limits when $m_N \gtrsim 100 \text{ GeV}$. Compared with current LHC limits, the FCC-eh gives more stringent limits when $m_N > 15 \text{ GeV}$ and are much stronger when $m_N \gtrsim 100 \text{ GeV}$.

The LNV signal process considered in this study is one typical channel to search for heavy Majorana neutrinos at electron-proton colliders. If this signal is discovered at colliders, it is also confirmed that the nature of N is of Majorana type. Therefore, our results are an important complement to the physics goals of electron-proton colliders, and the parameter space probed by our search strategy could explain other fundamental physics problems, such as the leptogenesis [67].

We assume that N decays promptly in this study. However, when N 's lifetime is long enough, heavy neutrinos can have sizeable probability to travel through and decay outside the detector. In this case, such neutrinos will be mis-detected and behave as missing energy, and thus these events cannot contribute to our signal. The number of detectable signal events needs to be multiplied by the average probability \bar{P} of heavy neutrinos decaying inside the detector's fiducial volume. Because our signal final state has one μ^+ and two jets from the the decay of N , in order to detect these jets, the heavy neutrino needs to decay before the end of the hadronic calorime-

ter (HCAL).

To estimate this effect on final limits, we consider detector layouts of the LHeC and FCC-eh from Ref. [68] and Ref. [69], respectively. We generate the signal sample $pe^- \rightarrow jN$ at the parton level using MadGraph for different m_N at the LHeC and FCC-eh, and calculate \bar{P} of detectors using a similar method used in Ref. [70]. Results for \bar{P} while varying $|V_{\ell N}|^2$ when $m_N = 5, 10, 20$ GeV at the LHeC and FCC-eh are derived, and we find that the resulting curves of detectors at LHeC and FCC-eh are very similar. For $m_N = 5, 10, 20$ GeV, the \bar{P} values begin to reduce from unity when the mixing parameter $|V_{\ell N}|^2 \sim 2 \times 10^{-6}, 3 \times 10^{-8}, 8 \times 10^{-10}$, respectively, and become zero when $|V_{\ell N}|^2 \sim 2 \times 10^{-9}, 5 \times 10^{-11}, 1 \times 10^{-12}$, respectively. Since Fig. 5 shows that the $2\text{-}\sigma$ upper limits on $|V_{\ell N}|^2$ for $m_N = 10$ GeV at the LHeC and FCC-eh are 7.8×10^{-5} and 9.0×10^{-6} , respectively, which are larger than 3×10^{-8} , the corresponding \bar{P} values are unity, and thus the final limits are not modified. For larger m_N , $|V_{\ell N}|^2$ is required to be even smaller such that \bar{P} can decrease from unity. Therefore, the effect of long-lived cases of heavy neutrinos is expected to be negligible for the mass range considered in this study. Such effect becomes significant for very small masses, and we leave it for future studies.

We note that when $|V_{eN}|^2 = |V_{\mu N}|^2$ the LNV signal $pe^- \rightarrow e^+jjj$ also exists with cross section approximately equal to that of signal $pe^- \rightarrow \mu^+jjj$. However, for the signal $pe^- \rightarrow e^+jjj$, there exists one additional SM background process of $pe^- \rightarrow e^-jjj$. When the final state e^- is mis-detected as e^+ , this process can be one significant background. To estimate sensitivities on $|V_{\ell N}|^2$ of the e^+ final state signal, we consider its corresponding SM background processes. The cross sections of background processes of $e^-jjj, e^+e^-e^-jjj, e^+e^-\nu_ejjj$ and $e^+\nu_e\nu_ejjj$ are found to be $1.4 \times 10^4, 0.53, 0.33$ and 8.1×10^{-6} pb at the LHeC, respectively. One sees that the production cross section of e^-jjj is much larger than the other background processes. Therefore, it could still dominate even if the detector's charge misidentification rate is small.

With the current detector configuration at the LHeC, after selecting exactly one positron with transverse momentum above 5 GeV, the total background cross section for the e^+ final state is 8.62×10^{-2} pb, among which the e^-jjj process is 6.07×10^{-2} pb and the sum of the other three background processes is 2.55×10^{-2} pb, so e^-jjj is the main background. For the μ^+ final state, the total background cross section after selecting exactly one muon with positive charge with transverse momentum above 5 GeV is 2.58×10^{-2} pb (cf. cut(i) in Table II).

Because the total background cross section for the e^+ final state is about three times larger than that for the μ^+ final state, the limit on mixing parameter $|V_{\ell N}|^2$ from the signal process $pe^- \rightarrow e^+jjj$ is expected to be weaker than that from the signal process $pe^- \rightarrow \mu^+jjj$. However, when $|V_{eN}|^2 \neq 0$ and $|V_{\mu N}|^2 = 0$, the $pe^- \rightarrow \mu^+jjj$ signal cannot be produced any more, but the $pe^- \rightarrow e^+jjj$ signal can still exist. Because the $pe^- \rightarrow e^+jjj$ signal process depends on the mixing parameter $|V_{eN}|^2$ only, it can be a unique channel to probe $|V_{eN}|^2$ independent of other mixing parameters. In this sense, the detailed analyses of the e^+ final state are still meaningful and we leave it for future studies.

Appendix A: Distributions of BDT responses

In Fig. 6 and Fig. 7, we show the distributions of BDT responses of the signal and SM background processes at the LHeC and FCC-eh with different m_N assumptions.

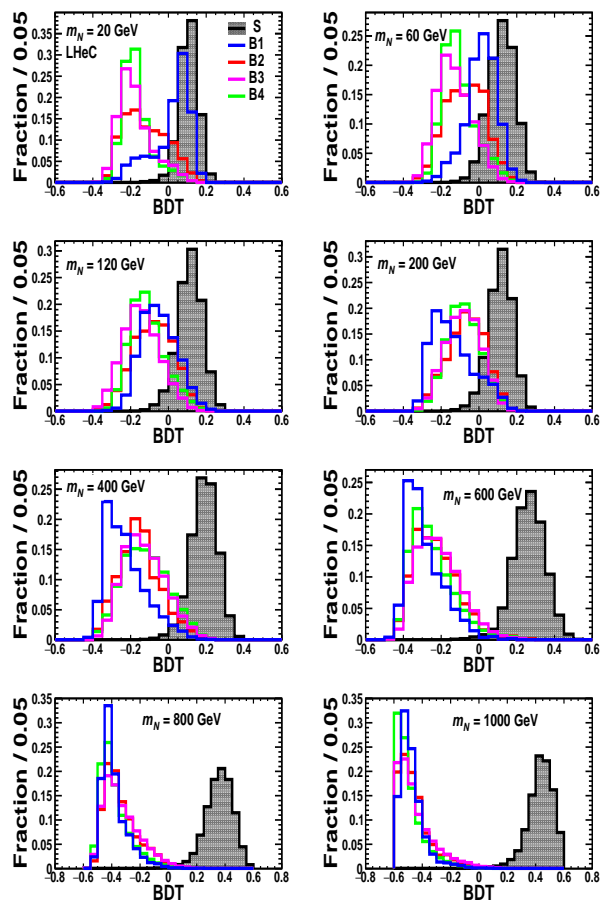


FIG. 6: Distributions of BDT responses of the signal (black, filled) and four background processes at the LHeC for representative heavy neutrino masses.

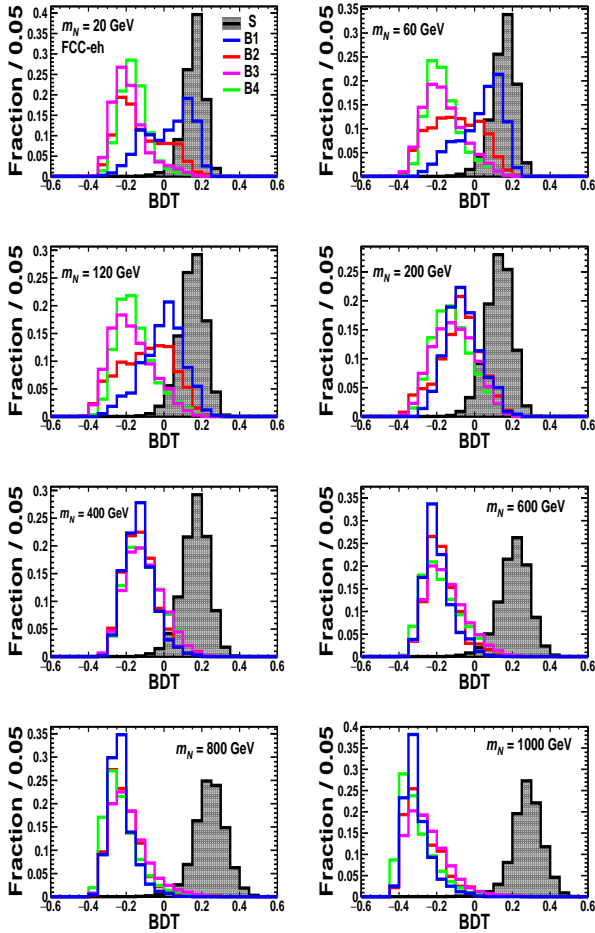


FIG. 7: The BDT distributions of the same processes as in Fig. 6, but at the FCC-eh.

Appendix B: Distributions of representative high-level observables

The following twenty-nine high-level observables are constructed and input to the TMVA package to perform the MVA-BDT analysis.

- The transverse momentum p_T , the energy E , the pseudorapidity η and the azimuthal angle ϕ of the final state particles: $E(\mu)$, $E(j_1)$, $E(j_2)$, $E(j_3)$, $p_T(\mu)$, $p_T(j_1)$, $p_T(j_2)$, $p_T(j_3)$, $\eta(\mu)$, $\eta(j_1)$, $\eta(j_2)$, $\eta(j_3)$, $\phi(\mu)$, $\phi(j_1)$, $\phi(j_2)$, $\phi(j_3)$.
- The number of jets $N(j)$ and the magnitude and the azimuthal angle of the missing transverse momentum: \cancel{E}_T , $\phi(\cancel{E}_T)$.
- p_T , η and ϕ of the system of $(j_2 + j_3)$: $p_T(j_2 + j_3)$, $\eta(j_2 + j_3)$, $\phi(j_2 + j_3)$.

- The pseudorapidity difference $\Delta\eta$, the azimuthal angle difference $\Delta\phi$ and the angular distance difference $\Delta R = \sqrt{(\Delta\eta)^2 + (\Delta\phi)^2}$ between the muon and jet(s): $\Delta\eta(\mu, j_1)$, $\Delta\eta(\mu, j_2 + j_3)$, $\Delta\phi(\mu, j_1)$, $\Delta\phi(\mu, j_2 + j_3)$, $\Delta R(\mu, j_1)$, $\Delta R(\mu, j_2 + j_3)$.
- The invariant mass M of the system of $(\mu + j_2 + j_3)$: $M(\mu + j_2 + j_3)$.

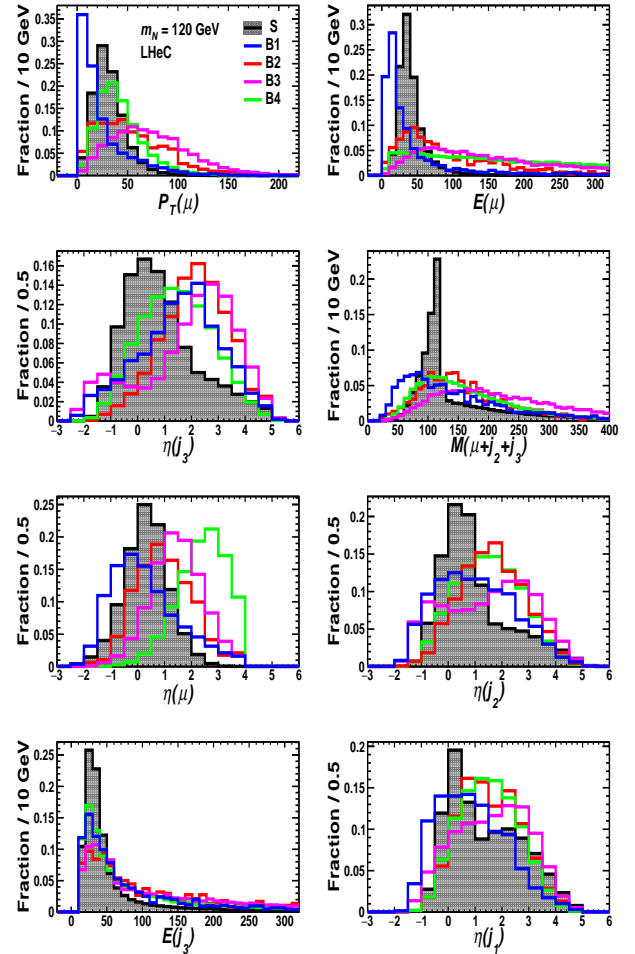
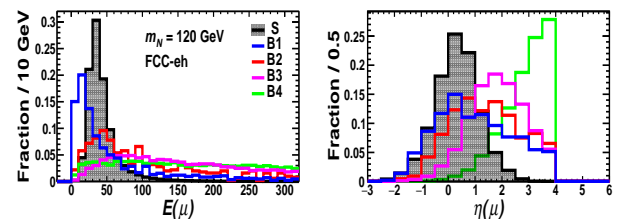


FIG. 8: Distributions of representative high-level observables for the signal with $m_N = 120$ GeV (black, filled) and four background processes at the LHeC.



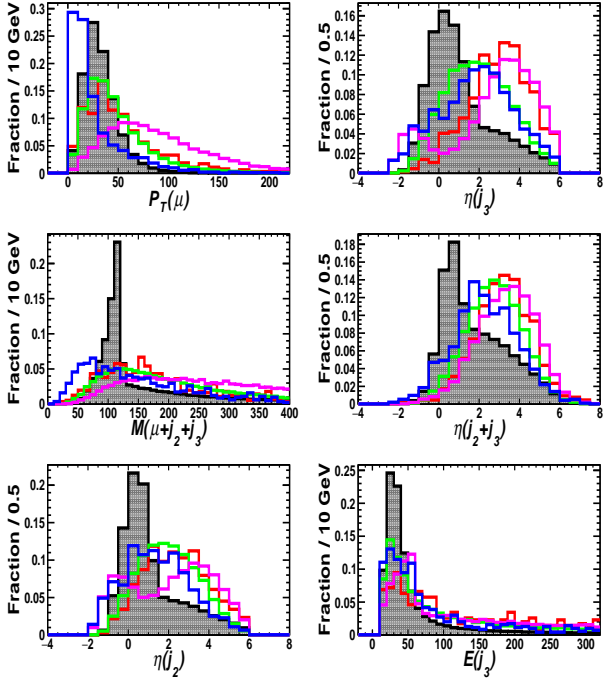


FIG. 9: The distributions of the same observables as in Fig. 8, but at the FCC-eh.

Appendix C: The Selection efficiency table

In Table III, we present selection efficiencies of pre-selection and BDT cuts for both signal and background processes at the LHeC and FCC-eh for representative heavy neutrino masses.

m_N	collider	selection	signal	$\mu^+\mu^-e^-jjj$	$\mu^+\mu^-\nu_ejjj$	$\mu^+\nu_\mu e^-jjj$	$\mu^+\nu_\mu\nu_ejjj$
20 GeV	LHeC	pre-selection	8.04×10^{-2}	1.63×10^{-3}	1.29×10^{-4}	7.07×10^{-4}	1.07×10^{-2}
		BDT>0.070	8.53×10^{-1}	4.57×10^{-1}	7.61×10^{-2}	2.00×10^{-2}	1.59×10^{-2}
	FCC-eh	pre-selection	1.20×10^{-1}	6.10×10^{-4}	1.22×10^{-4}	7.86×10^{-4}	4.71×10^{-3}
		BDT>0.112	8.25×10^{-1}	3.13×10^{-1}	4.54×10^{-2}	1.04×10^{-2}	7.52×10^{-3}
40 GeV	LHeC	pre-selection	2.40×10^{-1}	1.63×10^{-3}	1.29×10^{-4}	7.07×10^{-4}	1.07×10^{-2}
		BDT>0.125	4.76×10^{-1}	6.99×10^{-2}	1.62×10^{-2}	2.69×10^{-3}	5.30×10^{-3}
	FCC-eh	pre-selection	2.77×10^{-1}	6.10×10^{-4}	1.22×10^{-4}	7.86×10^{-4}	4.71×10^{-3}
		BDT>0.109	6.55×10^{-1}	3.07×10^{-1}	4.13×10^{-2}	8.75×10^{-3}	7.64×10^{-3}
60 GeV	LHeC	pre-selection	3.71×10^{-1}	1.63×10^{-3}	1.29×10^{-4}	7.07×10^{-4}	1.07×10^{-2}
		BDT>0.116	5.43×10^{-1}	8.38×10^{-2}	2.88×10^{-2}	5.37×10^{-3}	1.19×10^{-2}
	FCC-eh	pre-selection	3.91×10^{-1}	6.10×10^{-4}	1.22×10^{-4}	7.86×10^{-4}	4.71×10^{-3}
		BDT>0.111	7.73×10^{-1}	3.01×10^{-1}	4.40×10^{-2}	1.07×10^{-2}	1.39×10^{-2}
120 GeV	LHeC	pre-selection	5.66×10^{-1}	1.20×10^{-3}	1.08×10^{-4}	5.53×10^{-4}	9.07×10^{-3}
		BDT>0.067	7.71×10^{-1}	1.21×10^{-1}	8.36×10^{-2}	2.29×10^{-2}	4.74×10^{-2}
	FCC-eh	pre-selection	5.45×10^{-1}	4.53×10^{-4}	1.08×10^{-4}	6.64×10^{-4}	4.22×10^{-3}
		BDT>0.094	7.95×10^{-1}	1.72×10^{-1}	7.49×10^{-2}	1.63×10^{-2}	2.56×10^{-2}
200 GeV	LHeC	pre-selection	6.00×10^{-1}	1.20×10^{-3}	1.08×10^{-4}	5.53×10^{-4}	9.07×10^{-3}
		BDT>0.087	6.84×10^{-1}	4.10×10^{-2}	5.56×10^{-2}	3.01×10^{-2}	3.60×10^{-2}
	FCC-eh	pre-selection	5.57×10^{-1}	4.53×10^{-4}	1.08×10^{-4}	6.64×10^{-4}	4.22×10^{-3}
		BDT>0.102	6.59×10^{-1}	5.91×10^{-2}	4.37×10^{-2}	2.74×10^{-2}	2.74×10^{-2}
400 GeV	LHeC	pre-selection	4.33×10^{-1}	1.20×10^{-3}	1.08×10^{-4}	5.53×10^{-4}	9.07×10^{-3}
		BDT>0.154	6.98×10^{-1}	2.37×10^{-3}	7.05×10^{-3}	9.45×10^{-3}	9.63×10^{-3}
	FCC-eh	pre-selection	4.67×10^{-1}	4.53×10^{-4}	1.08×10^{-4}	6.64×10^{-4}	4.22×10^{-3}
		BDT>0.140	6.64×10^{-1}	3.28×10^{-3}	1.40×10^{-2}	1.26×10^{-2}	1.07×10^{-2}
600 GeV	LHeC	pre-selection	2.61×10^{-1}	1.20×10^{-3}	1.08×10^{-4}	5.53×10^{-4}	9.07×10^{-3}
		BDT>0.247	5.91×10^{-1}	–	1.76×10^{-3}	6.61×10^{-4}	5.33×10^{-4}
	FCC-eh	pre-selection	3.66×10^{-1}	4.53×10^{-4}	1.08×10^{-4}	6.64×10^{-4}	4.22×10^{-3}
		BDT>0.182	6.66×10^{-1}	–	–	3.43×10^{-3}	1.78×10^{-3}
800 GeV	LHeC	pre-selection	1.55×10^{-1}	1.20×10^{-3}	1.08×10^{-4}	5.53×10^{-4}	9.07×10^{-3}
		BDT>0.210	9.27×10^{-1}	–	–	1.12×10^{-3}	6.25×10^{-4}
	FCC-eh	pre-selection	2.57×10^{-1}	4.53×10^{-4}	1.08×10^{-4}	6.64×10^{-4}	4.22×10^{-3}
		BDT>0.211	6.71×10^{-1}	–	1.56×10^{-3}	2.08×10^{-3}	1.26×10^{-3}
1000 GeV	LHeC	pre-selection	7.92×10^{-2}	1.20×10^{-3}	1.08×10^{-4}	5.53×10^{-4}	9.07×10^{-3}
		BDT>0.238	9.63×10^{-1}	–	–	3.30×10^{-4}	5.51×10^{-5}
	FCC-eh	pre-selection	1.60×10^{-1}	4.53×10^{-4}	1.08×10^{-4}	6.64×10^{-4}	4.22×10^{-3}
		BDT>0.227	7.73×10^{-1}	–	1.56×10^{-3}	2.57×10^{-3}	1.15×10^{-3}

TABLE III: Selection efficiencies of pre-selection and BDT cuts for both signal and background processes at the LHeC and FCC-eh for representative heavy neutrino masses, where “–” means the number of events can be reduced to be negligible.

ACKNOWLEDGMENTS

We thank Lingxiao Bai, Marco Drewes, Filmon Andom Ghebretinsae, Ying-nan Mao, Minglun Tian and Zeren Simon Wang for helpful discussions. H.G. and K.W. are supported by the National Natural Science Foundation of China under grant no. 11905162, the Excellent Young

Talents Program of the Wuhan University of Technology under grant no. 40122102, and the research program of the Wuhan University of Technology under grant no. 2020IB024. The simulation and analysis work of this paper was completed with the computational cluster provided by the Theoretical Physics Group at the Department of Physics, School of Sciences, Wuhan University of Technology.

-
- [1] Super-Kamiokande, Y. Fukuda *et al.*, Evidence for oscillation of atmospheric neutrinos, *Phys. Rev. Lett.* **81**, 1562 (1998), arXiv:hep-ex/9807003, BU-98-17, ICRR-REPORT-422-98-18, UCI-98-8, KEK-PREPRINT-98-95, LSU-HEPA-5-98, UMD-98-003, SBHEP-98-5, TKU-PAP-98-06, TIT-HPE-98-09.
- [2] MINOS, D. G. Michael *et al.*, Observation of muon neutrino disappearance with the MINOS detectors and the NuMI neutrino beam, *Phys. Rev. Lett.* **97**, 191801 (2006), arXiv:hep-ex/0607088, FERMILAB-PUB-06-243, BNL-76806-2006-JA.
- [3] MINOS, P. Adamson *et al.*, Improved search for muon-neutrino to electron-neutrino oscillations in MINOS, *Phys. Rev. Lett.* **107**, 181802 (2011), arXiv:1108.0015, FERMILAB-PUB-11-351-PPD, BNL-96120-2011-JA.
- [4] Double Chooz Collaboration, Y. Abe *et al.*, Indication of reactor $\bar{\nu}_e$ disappearance in the double chooz experiment, *Phys. Rev. Lett.* **108**, 131801 (2012), <https://link.aps.org/doi/10.1103/PhysRevLett.108.131801>.
- [5] Daya Bay, J. Ling, Observation of electron-antineutrino disappearance at Daya Bay, *AIP Conf. Proc.* **1560**, 206 (2013).
- [6] S.-B. Kim, Observation of reactor electron antineutrino disappearance at RENO, *Nucl. Phys. B Proc. Suppl.* **235-236**, 24 (2013).
- [7] H. Fritzsch, M. Gell-Mann, and P. Minkowski, Vectorlike weak currents and new elementary fermions, *Physics Letters B* **59**, 256 (1975), <https://www.sciencedirect.com/science/article/pii/0370269375900404>.
- [8] P. Minkowski, $\mu \rightarrow e\gamma$ at a Rate of One Out of 10^9 Muon Decays?, *Phys. Lett.* **67B**, 421 (1977), Print-77-0182 (BERN).
- [9] T. Yanagida, Horizontal gauge symmetry and masses of neutrinos, *Proceedings: Workshop on the Unified Theories and the Baryon Number in the Universe*, *Conf. Proc.* **C7902131**, 95 (1979), KEK-79-18-95.
- [10] O. Sawada and A. Sugamoto, editors, *Proceedings: Workshop on the Unified Theories and the Baryon Number in the Universe: Tsukuba, Japan, February 13-14, 1979*, Tsukuba, Japan, 1979, Natl.Lab.High Energy Phys.
- [11] R. N. Mohapatra and G. Senjanovic, Neutrino Mass and Spontaneous Parity Nonconservation, *Phys. Rev. Lett.* **44**, 912 (1980), MDDP-TR-80-060, MDDP-PP-80-105, CCNY-HEP-79-10.
- [12] S. L. Glashow, The Future of Elementary Particle Physics, *NATO Sci. Ser. B* **61**, 687 (1980), HUTP-79-A059.
- [13] M. Gell-Mann, P. Ramond, and R. Slansky, Complex Spinors and Unified Theories, *Conf. Proc.* **C790927**, 315 (1979), PRINT-80-0576.
- [14] W.-Y. Keung and G. Senjanovic, Majorana Neutrinos and the Production of the Right-handed Charged Gauge Boson, *Phys. Rev. Lett.* **50**, 1427 (1983), BNL-32872.
- [15] R. Foot, H. Lew, X. G. He, and G. C. Joshi, Seesaw Neutrino Masses Induced by a Triplet of Leptons, *Z. Phys. C* **44**, 441 (1989), UM-P-88/89, OZ-P-88/7.
- [16] R. N. Mohapatra, Mechanism for Understanding Small Neutrino Mass in Superstring Theories, *Phys. Rev. Lett.* **56**, 561 (1986).
- [17] M. Magg and C. Wetterich, Neutrino mass problem and gauge hierarchy, *Physics Letters B* **94**, 61 (1980), <https://www.sciencedirect.com/science/article/pii/0370269380908254>.
- [18] A. Atre, T. Han, S. Pascoli, and B. Zhang, The Search for Heavy Majorana Neutrinos, *JHEP* **05**, 030 (2009), arXiv:0901.3589, FERMILAB-PUB-08-086-T, NSF-KITP-08-54, MADPH-06-1466, DCPT-07-198, IPPP-07-99.
- [19] F. F. Deppisch, P. S. Bhupal Dev, and A. Pilaftsis, Neutrinos and Collider Physics, *New J. Phys.* **17**, 075019 (2015), arXiv:1502.06541, MAN-HEP-2014-15.
- [20] A. Das and N. Okada, Improved bounds on the heavy neutrino productions at the LHC, *Phys. Rev. D* **93**, 033003 (2016), arXiv:1510.04790.
- [21] Y. Cai, T. Han, T. Li, and R. Ruiz, Lepton Number Violation: Seesaw Models and Their Collider Tests, *Front.in Phys.* **6**, 40 (2018), arXiv:1711.02180, PITT-PACC-1712, IPPP-17-74, COEPP-MN-17-17.
- [22] A. Das, Y. Gao, and T. Kamon, Heavy neutrino search via semileptonic Higgs decay at the LHC, *Eur. Phys. J. C* **79**, 424 (2019), arXiv:1704.00881, WSU-HEP-1706, MI-TH-1748.

- [23] P. D. Bolton, F. F. Deppisch, and P. S. Bhupal Dev, Neutrinoless double beta decay versus other probes of heavy sterile neutrinos, *JHEP* **03**, 170 (2020), arXiv:1912.03058.
- [24] CMS, A. M. Sirunyan *et al.*, Search for heavy neutral leptons in events with three charged leptons in proton-proton collisions at $\sqrt{s} = 13$ TeV, *Phys. Rev. Lett.* **120**, 221801 (2018), arXiv:1802.02965, CMS-EXO-17-012, CERN-EP-2018-006.
- [25] CMS, A. M. Sirunyan *et al.*, Search for heavy Majorana neutrinos in same-sign dilepton channels in proton-proton collisions at $\sqrt{s} = 13$ TeV, *JHEP* **01**, 122 (2019), arXiv:1806.10905, CMS-EXO-17-028, CERN-EP-2018-159.
- [26] CMS, Search for long-lived heavy neutral leptons with displaced vertices in pp collisions at $\sqrt{s} = 13$ TeV with the CMS detector, (2021), CMS-PAS-EXO-20-009.
- [27] ATLAS, G. Aad *et al.*, Search for heavy neutral leptons in decays of W bosons produced in 13 TeV pp collisions using prompt and displaced signatures with the ATLAS detector, *JHEP* **10**, 265 (2019), arXiv:1905.09787, CERN-EP-2019-071.
- [28] LHCb, R. Aaij *et al.*, Search for heavy neutral leptons in $W^+ \rightarrow \mu^+ \mu^\pm \text{jet}$ decays, *Eur. Phys. J. C* **81**, 248 (2021), arXiv:2011.05263, LHCb-PAPER-2020-022, CERN-EP-2020-194.
- [29] NA62, E. Cortina Gil *et al.*, Search for heavy neutral lepton production in K^+ decays to positrons, *Phys. Lett. B* **807**, 135599 (2020), arXiv:2005.09575, CERN-EP-2020-089.
- [30] Belle, D. Liventsev *et al.*, Search for heavy neutrinos at Belle, *Phys. Rev. D* **87**, 071102 (2013), arXiv:1301.1105, [Erratum: *Phys.Rev.D* 95, 099903 (2017)], BELLE-PREPRINT-2012-28, KEK-PREPRINT-2012-32.
- [31] T2K, K. Abe *et al.*, Search for heavy neutrinos with the T2K near detector ND280, *Phys. Rev. D* **100**, 052006 (2019), arXiv:1902.07598.
- [32] SHiP, C. Ahdida *et al.*, Sensitivity of the SHiP experiment to Heavy Neutral Leptons, *JHEP* **04**, 077 (2019), arXiv:1811.00930.
- [33] M. Chraszcz *et al.*, A frequentist analysis of three right-handed neutrinos with GAMBIT, *Eur. Phys. J. C* **80**, 569 (2020), arXiv:1908.02302, gambit-physics-2019.
- [34] M. Klein, The Large Hadron Electron Collider Project, in *17th International Workshop on Deep-Inelastic Scattering and Related Subjects*, p. 236, 2009, arXiv:0908.2877.
- [35] LHeC Study Group, J. L. Abelleira Fernandez *et al.*, A Large Hadron Electron Collider at CERN: Report on the Physics and Design Concepts for Machine and Detector, *J. Phys. G* **39**, 075001 (2012), arXiv:1206.2913, SLAC-R-999, CERN-OPEN-2012-015, LHEC-NOTE-2012-001-GEN.
- [36] O. Bruening and M. Klein, The Large Hadron Electron Collider, *Mod. Phys. Lett. A* **28**, 1330011 (2013), arXiv:1305.2090, LHEC-NOTE-2013-001-GEN.
- [37] M. Klein, Deep inelastic scattering at the energy frontier, *Annalen Phys.* **528**, 138 (2016).
- [38] LHeC, FCC-he Study Group, P. Agostini *et al.*, The Large Hadron-Electron Collider at the HL-LHC, *J. Phys. G* **48**, 110501 (2021), arXiv:2007.14491, CERN-ACC-Note-2020-0002, JLAB-ACP-20-3180.
- [39] LHeC, FCC-eh Study Group, B. Holzer and K. D. J. André, Energy Frontier DIS at CERN: the LHeC and the FCC-eh, *PoS ICHEP2020*, 687 (2021).
- [40] F. Zimmermann, M. Benedikt, D. Schulte, and J. Wenninger, Challenges for Highest Energy Circular Colliders, in *5th International Particle Accelerator Conference*, p. MOXAA01, 2014.
- [41] R. Tomás *et al.*, Fcc study: parameters and optics for hadron and lepton colliders, *Nuclear and Particle Physics Proceedings* **273-275**, 149 (2016), 37th International Conference on High Energy Physics (ICHEP), <https://www.sciencedirect.com/science/article/pii/S2405601415005076>.
- [42] FCC, A. Abada *et al.*, FCC Physics Opportunities: Future Circular Collider Conceptual Design Report Volume 1, *Eur. Phys. J. C* **79**, 474 (2019), CERN-ACC-2018-0056.
- [43] LHeC/FCC-eh Study Group, G. Azuelos, M. D'Onofrio, and O. Fischer, Beyond Standard Model Physics at the LHeC and the FCC-eh, *PoS ICHEP2020*, 227 (2021).
- [44] W. Buchmüller and C. Greub, Electroproduction of majorana neutrinos, *Physics Letters B* **256**, 465 (1991), <https://www.sciencedirect.com/science/article/pii/037026939191792T>.
- [45] W. Buchmuller and C. Greub, Heavy Majorana neutrinos in electron - positron and electron - proton collisions, *Nucl. Phys. B* **363**, 345 (1991), DESY-91-034.
- [46] W. Buchmuller and C. Greub, Right-handed currents and heavy neutrinos in high-energy ep and e^+e^- scattering, *Nucl. Phys. B* **381**, 109 (1992), DESY-92-023, ZU-TH-9-92.
- [47] G. Ingelman and J. Rathsman, Heavy Majorana neutrinos at e p colliders, *Z. Phys. C* **60**, 243 (1993), DESY-93-039, TSL-ISV-93-0081.
- [48] H. Liang, X.-G. He, W.-G. Ma, S.-M. Wang, and R.-Y. Zhang, Seesaw Type I and III at the LHeC, *JHEP* **09**, 023 (2010), arXiv:1006.5534.
- [49] C. Blaksley, M. Blennow, F. Bonnet, P. Coloma, and E. Fernandez-Martinez, Heavy Neutrinos and Lepton Number Violation in lp Colliders, *Nucl. Phys. B* **852**, 353 (2011), arXiv:1105.0308, CERN-PH-TH-2011-094, EURONU-WP6-11-32, IFT-UAM-CSIC-11-25, MPP-2011-50.
- [50] L. Duarte, G. A. González-Sprinberg, and O. A. Sampayo, Majorana neutrinos production at LHeC in an effective approach, *Phys. Rev. D* **91**, 053007 (2015), arXiv:1412.1433.
- [51] S. Mondal and S. K. Rai, Probing the Heavy Neutrinos of Inverse Seesaw Model at the LHeC, *Phys. Rev. D* **94**,

- 033008 (2016), arXiv:1605.04508, HRI-RECAPP-2016-009.
- [52] S. Antusch, E. Cazzato, and O. Fischer, Sterile neutrino searches at future e^-e^+ , pp , and e^-p colliders, *Int. J. Mod. Phys. A* **32**, 1750078 (2017), arXiv:1612.02728.
- [53] M. Lindner, F. S. Queiroz, W. Rodejohann, and C. E. Yaguna, Left-Right Symmetry and Lepton Number Violation at the Large Hadron Electron Collider, *JHEP* **06**, 140 (2016), arXiv:1604.08596.
- [54] S.-Y. Li, Z.-G. Si, and X.-H. Yang, Heavy Majorana Neutrino Production at Future ep Colliders, *Phys. Lett. B* **795**, 49 (2019), arXiv:1811.10313.
- [55] A. Das, S. Jana, S. Mandal, and S. Nandi, Probing right handed neutrinos at the LHeC and lepton colliders using fat jet signatures, *Phys. Rev. D* **99**, 055030 (2019), arXiv:1811.04291, OSU-HEP-18-06.
- [56] S. Antusch, O. Fischer, and A. Hammad, Lepton-Trijet and Displaced Vertex Searches for Heavy Neutrinos at Future Electron-Proton Colliders, *JHEP* **03**, 110 (2020), arXiv:1908.02852.
- [57] G. Cottin, O. Fischer, S. Mandal, M. Mitra, and R. Padhan, Displaced Neutrino Jets at the LHeC, (2021), arXiv:2104.13578.
- [58] D. Alva, T. Han, and R. Ruiz, Heavy Majorana neutrinos from $W\gamma$ fusion at hadron colliders, *JHEP* **02**, 072 (2015), arXiv:1411.7305, PITT-PACC-1407.
- [59] C. Degrande, O. Mattelaer, R. Ruiz, and J. Turner, Fully-Automated Precision Predictions for Heavy Neutrino Production Mechanisms at Hadron Colliders, *Phys. Rev. D* **94**, 053002 (2016), arXiv:1602.06957, IPPP-16-13, MCNET-16-05.
- [60] J. Alwall *et al.*, The automated computation of tree-level and next-to-leading order differential cross sections, and their matching to parton shower simulations, *JHEP* **07**, 079 (2014), arXiv:1405.0301, CERN-PH-TH-2014-064, CP3-14-18, LPN14-066, MCNET-14-09, ZU-TH-14-14.
- [61] G. Azuelos, M. D’Onofrio, S. Iwamoto, and K. Wang, Search for the SUSY electroweak sector at ep colliders, *Phys. Rev. D* **101**, 095015 (2020), arXiv:1912.03823.
- [62] T. Sjostrand, S. Mrenna, and P. Z. Skands, PYTHIA 6.4 Physics and Manual, *JHEP* **05**, 026 (2006), arXiv:hep-ph/0603175, FERMILAB-PUB-06-052-CD-T, LU-TP-06-13.
- [63] LHeC and FCC-eh Delphes card files, https://github.com/delphes/delphes/blob/master/cards/delphes_card_LHeC.tcl, https://github.com/delphes/delphes/blob/master/cards/delphes_card_FCCeh.tcl.
- [64] DELPHES 3, J. de Favereau *et al.*, DELPHES 3, A modular framework for fast simulation of a generic collider experiment, *JHEP* **02**, 057 (2014), arXiv:1307.6346.
- [65] H1 and ZEUS, R. Placakyte, Parton Distribution Functions, in *31st International Symposium on Physics In Collision*, 2011, arXiv:1111.5452.
- [66] A. Hocker *et al.*, TMVA - Toolkit for Multivariate Data Analysis, (2007), arXiv:physics/0703039, CERN-OPEN-2007-007.
- [67] M. Drewes, Y. Georis, and J. Klarić, Mapping the Viable Parameter Space for Testable Leptogenesis, *Phys. Rev. Lett.* **128**, 051801 (2022), arXiv:2106.16226, CP3-21-43.
- [68] J. L. Abelleira Fernandez *et al.*, A Large Hadron Electron Collider at CERN, in *CERN Council Open Symposium on European Strategy for Particle Physics*, 2012, arXiv:1211.4831.
- [69] A. Polini, The FCC-eh Detector, in *FCC Week 2021*, 2021, <https://indico.cern.ch/event/995850/contributions/4420316/attachments/2273829/3862232/2021-06-30-AP-FCC.pdf>.
- [70] Z. S. Wang and K. Wang, Long-lived light neutralinos at future Z -factories, *Phys. Rev. D* **101**, 115018 (2020), arXiv:1904.10661, BONN-TH-2019-01.